Journal of Solid Mechanics Vol. 3, No. 1 (2011) pp. 19-41

Mechanical and Thermal Stresses in a FGPM Hollow Cylinder Due to Non-Axisymmetric Loads

M. Jabbari[1,*], M. Meshkini[1], M.R. Eslami[2]

[1]*South Tehran Branch, Islamic Azad University, Iran*
[2]*Department of Mechanical Engineering, Amirkabir University of Technology, Iran*

Received 25 December 2010; accepted 15 February 2011

ABSTRACT

In this paper, the general solution of steady-state two-dimensional non-axisymmetric mechanical and thermal stresses and mechanical displacements of a hollow thick cylinder made of fluid-saturated functionally graded porous material (FGPM) is presented. The general form of thermal and mechanical boundary conditions is considered on the inside and outside surfaces. A direct method is used to solve the heat conduction equation and the non-homogenous system of partial differential Navier equations, using the Complex Fourier Series and the power law functions method. The material properties, except of Poisson's ratio, are assumed to depend on the radial variable *r* and they are expressed as power law functions.

Keywords: Hollow cylinder; Non-homogenous; Non-axisymmetric; FGPM; Navier equations.

1 INTRODUCTION

FUNCTIONALLY graded materials (FGMs) are heterogeneous materials in which the elastic and thermal properties change from one surface to the other, gradually and continuously .The material is constructed by smoothly changing materials. Since ceramic has good heat resistance and metal has high strength, ceramic-Metal FGM may work at super high-temperatures or under high-temperatures difference field. In effect, the governing equation for the temperature and stress distributions are coordinate dependent as the material properties are functions of position. Classical method of analysis is to combine the equilibrium equations with the stress-strain and strain-displacement relations to arrive at the governing equation in terms of the displacement components called the Navier equation. There are some analytical thermal and stress calculations for functionally graded material in the on-dimensional case for thick cylinders and spheres [1, 2] the authors have considered the non-homogeneous material properties as liner function of r.

Jabbari et al.[3] studied a general solution for mechanical and thermal stresses in a functionally graded hollow cylinder due to non-axisymmetric steady-state load They applied separation of variables and Complex Fourier Series to solve the heat conduction and Navier equation. Poultangari et al.[4]presented Functionally graded hollow spheres under non-axisymmetric thermo-mechanical loads. Shariyat et al. [5] presented nonlinear transient thermal stress and elastic wave propagation analyses of thick temperature-dependent FGM cylinders, using a second-order point-collocation method. Lü Chen and Lim [6] presented elastic mechanical behavior of nano-scaled FGM films incorporating surface energies. Afsar, Sekine [7] presented inverse problems of material distributions for prescribed apparent fracture toughness in FGM coatings around a circular hole in infinite elastic media. Da-Guang Zhang, You-He Zhou [8] presented a theoretical analysis of FGM thin plates based on physical neutral surface. Fazelzadeh and Hosseini [9] presented aerothermoelastic behavior of supersonic rotating thin-walled beams made of functionally graded materials. Ootao and Tanigawa [10] presented the transient thermo elastic problem of

* Corresponding author. Tel.: +98 21 22217158; Fax: +98 21 22211088
E-mail address: *m_ jabbari@azad.ac.ir* (M. Jabbari).

functionally graded thick strip due to non-uniform heat supply. They obtained the exact solution for the two-dimensional temperature change in a transient state, and thermal stresses of a simple supported strip under the state of plane strain. Jabbari et al. [11] presented studied the mechanical and thermal stresses in functionally graded hollow cylinder due to radial symmetric loads. They assumed the temperature distribution to be a function of radial direction. They applied a method to solve the heat conduction and Navier equations. Farid et al. [12] presented three-dimensional temperature dependent free vibration analysis of functionally graded material curved panels resting on two-parameter elastic foundation using a hybrid semi-analytic, differential quadrature method. Bagri and Eslami [13] presented generalized coupled thermo elasticity of functionally graded annular disk considering the Lord–Shulman theory. Samsam et al. [14] presented buckling of thick functionally graded plates under mechanical and thermal loads. Jabbari et al [15] studied an axisymmetric mechanical and thermal stresses in thick short length functionally graded material cylinder. They applied separation of variables and Complex Fourier series to solve the heat conduction and Navier equation. Thieme et al. [16] presented Titanium powder sintering for preparation of a porous FGM destined as a skeletal replacement implant.

Poroelasticity is a theory that models the interaction of deformation and fluid flow in a fluid-saturated porous medium. The deformation of the medium influences the flow of the fluid and vice versa .The theory was proposed by Biot [17, 18] as a theoretical extension of soil consolidation models developed to calculate the settlement of structurdes placed on fluid-saturated porous soils. The historical development of the theory is sketched by Boer [19]. The theory has been widely applied to geotechnical problems beyond soil consolidation, most notable problems in rock mechanics. Detournay and Cheng [20] surveyed both these methods with special attention to rock mechanics. These include familiar analytical methods (displacement potentials, method of singularities) and computational methods (finite element and boundary element). Sandhu and Wilson [21] studied the application of finite element techniques to poroelasticity. Detournay and Cheng [22] presented fundamentals of poroelasticity. Abousleiman and Ekbote [23] presented the analytical solutions for inclining hollow cylinder in a transversely isotropic material subjected to thermal and stress perturbations, and they systematically evaluated the effect of the anisotropy of the poromechanical material parameters as well as thermal material properties on stress and porous pressure distributions. Chen [24] presented analyzed the problems of linear thermo elasticity in a transversely isotropic hollow cylinder of finite length by a direct power series approximation through the application of the Lanczos-Chebyshev method. Bai [25] presented then derived an analytical method solving the responses of a saturated porous media subjected to cyclic thermal loading by the Laplace transform and the Gauss-Lengender method of Laplace transform inversion. Wang and Papamichos [26, 27] presented analytical solution for the temperature, pore pressure and stresses around a cylindrical well bored and a spherical cavity subjected to a constant fluid flow rate by coupling the conductive heat transfer with the pore-fluid flow. Ghassemi and Tao [28] presented influence of coupled chemo-poro-thermoelastic processes on pore pressure and stress distributions around a wellbore in swelling shale. Beneikt and sobey [29] presented an-axisymmetric and fully 3-D poroelasticmodel forth evolution of hydrocephalus. Yang and Zhang [30] presented poroelastic wave equation including the Biot /squirt mechanism and the solid/fluid coupling anisotropy .Arora and Tomar [31] presented the elastic waves along a cylindrical borehole in a poroelastic medium saturated by two immiscible fluids. Hamiel [32] presented the coupled evolution of damage and porosity in poroelastic media theory and applications to deformation of porous rocks. Ghassemi [33] presented stress and pore pre pressure distribution around a pressurized, cooled crack in hollow permeability rock. Youssef [34] theory of generalized porothermoelasticity presented. Jourine et.al [35] presented Modeling poroelastic hollow cylinder experiments with realistic boundary conditions.

In this work, an analytical method is presented for mechanical and thermal stress analysis for a hollow cylinder made of fluid saturated porous functionally graded materials. Temperature distribution is considered in steady state non-axisymmetric case and mechanical and thermal boundary conditions are considered in general forms. At the end, the effects of graded changing and porosity are investigated on stresses.

2 EQUATIONS

2.1 Heat conduction problem

Consider a hollow circular cylinder of inner radius and outer radius made of FGPM (Functionally Graded Porous Material), respectively. Non axisymmtric cylindrical coordinates (r,θ) are considered along the radial and circumferential direction, respectively. The cylinder's material graded through the *r*-direction. Thus, the material properties are porous and functions *r*. The first law of thermodynamics for energy equation in the steady-state condition for the FGPM two dimensional cylinders is [3]

$$\frac{\partial^2 T}{\partial r^2}+\left(\frac{k'(r)}{k(r)}+\frac{1}{r}\right)\frac{\partial T}{\partial r}+\frac{1}{r^2}\frac{\partial^2 T}{\partial \theta^2}=0, \qquad a\le r\le b, \qquad -\pi\le\theta\le+\pi \tag{1}$$

where $T(r,\theta)$ is temperature distribution, $k(r)$ is the thermal conduction coefficient. The thermal boundary are assumed as:

$$\begin{aligned} &S_{11}T(a,\theta)+S_{12}T_{,r}(a,\theta)=f_1(\theta)\\ &S_{21}T(b,\theta)+S_{22}T_{,r}(b,\theta)=f_2(\theta)\end{aligned} \tag{2}$$

where S_{ij} are the constant thermal parameters related to conduction and convection coefficients. The functions $f_1(\theta)$ and $f_2(\theta)$ are known as the inner and outer radii, respectively. We assume that non-homogeneous thermal conduction coefficient $k(r)$ is power function of r as $k(r)=k_0 r^{m_3}$. Using the definition for the material properties, the temperature equation becomes:

$$\frac{\partial^2 T}{\partial r^2}+(m_3+1)\frac{1}{r}\frac{\partial T}{\partial r}+\frac{1}{r^2}\frac{\partial^2 T}{\partial \theta^2}=0 \tag{3}$$

The solution of Eq. (3) is written in the form of Complex Fourier Series, as [3]

$$T(r,\theta)=\sum_{n=-\infty}^{\infty}T_n(r)e^{in\theta} \tag{4}$$

Substituting Eq. (4) into Eq. (3), the following equation is obtained

$$\frac{d^2T_n(r)}{dr^2}+(m_3+1)\frac{1}{r}\frac{dT_n(r)}{dr}-\frac{n^2}{r^2}T_n(r)=0 \tag{5}$$

Eq. (6) is the Euler equation and has solutions in the form of [3]

$$T_n(r)=A_n r^{\beta} \tag{6}$$

Substituting Eq. (6) into Eq. (5), the following characteristic equation is obtained:

$$\beta^2+m_3\beta-n^2=0 \tag{7}$$

The roots of Eq. (7) are:

$$\beta_{n1,2}=\frac{-m_3}{2}\mp\left(\frac{m_3^2}{4}+n^2\right)^{1/2} \tag{8}$$

Thus:

$$T_n(r)=A_{n1}r^{\beta_{n1}}+A_{n2}r^{\beta_{n2}} \tag{9}$$

Substituting Eq. (9) into Eq. (4) gives:

$$T(r,\theta)=\sum_{n=-\infty}^{\infty}(A_{n1}r^{\beta_{n1}}+A_{n2}r^{\beta_{n2}})e^{in\theta} \tag{10}$$

The constants A_{n1} and A_{n2} are presented at Appendix B.

2.2 Stress analysis

Let u and v be displacement components in the radial and circumferential directions, respectively. Then, strain-displacement relations are [3]

$$\varepsilon_{rr}=\frac{\partial u}{\partial r},\qquad \varepsilon_{\theta\theta}=\frac{1}{r}\frac{\partial v}{\partial r}+\frac{u}{r},\qquad \varepsilon_{r\theta}=\frac{1}{2}\left(\frac{1}{r}\frac{\partial u}{\partial \theta}+\frac{\partial v}{\partial r}-\frac{v}{r}\right) \tag{11}$$

Stress-strain relations of a FGPM cylinder for non-axisymmtric condition are [3]

$$\begin{aligned}\sigma_{rr}&=C_{11}\varepsilon_{rr}+C_{12}\varepsilon_{\theta\theta}+e_{21}E_r-\gamma\, p\delta_{rr}-Z_1T(r,\theta)\\ \sigma_{\theta\theta}&=C_{22}\varepsilon_{\theta\theta}+C_{12}\varepsilon_{rr}+e_{22}E_r-\gamma\, p\delta_{\theta\theta}-Z_2T(r,\theta)\\ \sigma_{r\theta}&=2C_{66}\varepsilon_{r\theta}-e_{26}E_\theta-\gamma\, p\delta_{r\theta}+\lambda\in\delta_{r\theta}\end{aligned} \tag{12}$$

where σ_{ij}, ε_{ij} $(i,j=r,\theta)$, C_{ij}, M, γ, α, and μ are stress tensor, strain tensor, elastic constant, Biot's modulus, Biot's coefficient of effective stress, thermal expansion coefficient and Lame's coefficient, respectively.

$$M=\frac{2\mu(\nu_u-\nu)}{\gamma^2(1-2\nu)(1-2\nu_u)} \tag{13}$$

$$C_{11}+M\gamma^2=\overset{*}{C}_{11},\qquad C_{22}+M\gamma^2=\overset{*}{C}_{22},\qquad C_{12}+M\gamma^2=\overset{*}{C}_{12},\qquad C_{66}=\overset{*}{C}_{66} \tag{14}$$

Thus:

$$\begin{aligned}\sigma_{rr}&=\overset{*}{C}_{11}\,\varepsilon_{rr}+\overset{*}{C}_{12}\,\varepsilon_{\theta\theta}+e_{21}E_r-Z_1T(r,\theta)\\ \sigma_{\theta\theta}&=\overset{*}{C}_{12}\,\varepsilon_{rr}+\overset{*}{C}_{22}\,\varepsilon_{\theta\theta}+e_{22}E_r-Z_2T(r,\theta)\\ \sigma_{r\theta}&=2\overset{*}{C}_{66}\,\varepsilon_{r\theta}-e_{26}E_\theta\end{aligned} \tag{15}$$

where:

$$Z_1=\overset{*}{C}_{11}\,\alpha_r+2\overset{*}{C}_{12}\,\alpha_\theta \tag{16}$$

$$Z_2=2\overset{*}{C}_{12}\,\alpha_r+\overset{*}{C}_{22}\,\alpha_\theta \tag{17}$$

The equilibrium equations in the radial and circumferential direction, disregarding the body force and the inertia terms are

$$\begin{aligned}&\frac{\partial\sigma_{rr}}{\partial r}+\frac{1}{r}\frac{\partial\sigma_{r\theta}}{\partial\theta}+\frac{1}{r}(\sigma_{rr}-\sigma_{\theta\theta})=0\\ &\frac{\partial\sigma_{r\theta}}{\partial r}+\frac{1}{r}\frac{\partial\sigma_{\theta\theta}}{\partial\theta}+\frac{2}{r}(\sigma_{r\theta})=0\end{aligned} \tag{18}$$

To obtain the equilibrium equations in terms of the displacement components for the FGPM cylinder, the functional relationship of the material properties must be known. Because the cylinder material is assumed to be graded along the r-direction, the modulus of elasticity and coefficient of thermal expansion are assumed to be described with the power laws as

$$\alpha_r = \alpha_{01} r^{m_1}, \qquad \alpha_\theta = \alpha_{02} r^{m_2}, \qquad K = k_0 r^{m_3}, \qquad \overset{*}{C}_{ij} = \bar{C}_{ij} r^{m4} \tag{19}$$

where the coefficients are described as:

$$\alpha_{01} = \frac{\alpha_{01}'}{a^{m_1}}, \qquad \alpha_{02} = \frac{\alpha_{02}{}'}{a^{m_2}}, \qquad K = \frac{k_0{}'}{a^{m_3}}, \qquad \bar{C}_{ij} = \frac{\bar{C}_{ij}{}'}{a^{m4}} \tag{20}$$

and a is the inner radius. Using the relations (11) to (20) the Navier equations in terms of the displacement components are:

$$\begin{aligned}
&\left[\frac{\partial^2 u}{\partial r^2} + (m_4+1)\frac{1}{r}\left(\frac{\partial u}{\partial r}\right) + \left(\frac{(m_4+1)\bar{C}_{12} - \bar{C}_{22}}{\bar{C}_{11}}\right)\frac{1}{r^2}u + \left(\frac{\bar{C}_{66}}{\bar{C}_{11}}\right)\frac{1}{r^2}\frac{\partial^2 u}{\partial^2 \theta} + \left(\frac{\bar{C}_{12}+\bar{C}_{66}}{\bar{C}_{11}}\right)\frac{1}{r}\frac{\partial^2 v}{\partial r \partial \theta} + \left[\frac{m_4\bar{C}_{12} - \bar{C}_{22} - \bar{C}_{66}}{\bar{C}_{11}}\right]\frac{1}{r^2}\frac{\partial v}{\partial \theta}\right] r^{m_4} \\
&\quad = \left\{\left\{\left[\frac{(m_1+m_4-1)\bar{C}_{11} - 2\bar{C}_{12}}{\bar{C}_{11}}\right] r^{m_1-1}\alpha_{01} + \left[\frac{2(m_2+m_4+1)\bar{C}_{12} + \bar{C}_{22}}{\bar{C}_{11}}\right] r^{m_2-1}\alpha_{02}\right\} T(r,\theta) + \left[\frac{\bar{C}_{11} r^{m_1}\alpha_{01} + 2\bar{C}_{12} r^{m_2}\alpha_{02}}{\bar{C}_{11}}\right]\frac{dT}{dr}\right\} r^{m_4} \\
&\left[(\bar{C}_{66})\frac{\partial^2 v}{\partial r^2} + \left[(m_4+1)\bar{C}_{66}\right]\frac{1}{r}\cdot\frac{\partial v}{\partial r} - \left[(m_4+1)\bar{C}_{66}\right]\frac{1}{r^2}v + [\bar{C}_{22}]\frac{1}{r^2}\frac{\partial^2 v}{\partial \theta^2} + (\bar{C}_{66}+\bar{C}_{12})\frac{1}{r}\cdot\frac{\partial^2 u}{\partial r \partial \theta} + \left[(m_4+1)\bar{C}_{44} + \bar{C}_{12}\right]\frac{1}{r^2}\frac{\partial u}{\partial \theta}\right] * r^{m_4} \\
&\quad = \left[(2\bar{C}_{12}\alpha_{01} r^{m_1} + \bar{C}_{22}\alpha_{02} r^{m_2})\frac{1}{r}\frac{\partial T}{\partial \theta}\right] r^{m_4}
\end{aligned} \tag{21}$$

The Naviear Eqs. (21) are non-homogeneous system of partial differential equations with non-constant coefficients. For simplicity of analysis, we consider the power law of material properties to be the same as $m_1 = m_2 = m_4$.

2.3 Solution of the Navier equation

$$u(r,\theta) = \sum_{n=-\infty}^{\infty} u_n(r)\, \mathrm{e}^{in\theta}, \qquad v(r,\theta) = \sum_{n=-\infty}^{\infty} v_n(r)\, \mathrm{e}^{in\theta} \tag{22}$$

Substituting Eq. (11) and Eq. (22) into Eqs. (21) yield:

$$\begin{aligned}
&u_n'' + (m_4+1)\frac{1}{r}u_n' + \left(\frac{(m_4+1)\bar{C}_{12} - \bar{C}_{22} - n^2\bar{C}_{66}}{\bar{C}_{11}}\right)\frac{1}{r^2}u_n + in\left(\frac{\bar{C}_{12}+\bar{C}_{66}}{\bar{C}_{11}}\right)\frac{1}{r}.v_n' + in\left(\frac{m_4\bar{C}_{12} - \bar{C}_{22} - \bar{C}_{66}}{\bar{C}_{11}}\right)\frac{1}{r^2}v_n \\
&\quad = \left\{\left[\left(m_2 + m_4 - 1 - \frac{2\bar{C}_{12}}{\bar{C}_{11}}\right)\alpha_{01} + \left(\frac{2(m_2+m_4+1)\bar{C}_{12} + \bar{C}_{22}}{\bar{C}_{11}}\right)\alpha_{02}\right]\left[A_{n_1} r^{\beta_{n1}+m_2-1} + A_{n2} r^{\beta_{n2}+m_2-1}\right]\right. \\
&\qquad \left. + \left(\alpha_{01} + \frac{2\bar{C}_{12}}{\bar{C}_{11}}\alpha_{02}\right)\left[\beta_{n1} A n_1 r^{\beta_{n1}-m_2-1} + \beta_{n2} A_{n2} r^{\beta_{n2}+m_2-1}\right]\right\} \\
&v_n'' + (m_4+1)\frac{1}{r}v_n' - \left[(m_4+1) + \frac{n^2\bar{C}_{22}}{\bar{C}_{66}}\right]\frac{1}{r^2}v_n + in\left(\frac{\bar{C}_{12}}{\bar{C}_{66}} + 1\right)\frac{1}{r}u_n' + in\left((m_4+1) + \frac{\bar{C}_{12}}{\bar{C}_{66}}\right)\frac{1}{r^2}u_n \\
&\quad = \left\{\left[in\left(\frac{2\bar{C}_{12}}{\bar{C}_{66}}\right)\alpha_{01} + \frac{in\bar{C}_{22}}{\bar{C}_{66}}\alpha_{02}\right]\left[An_1 r^{\beta_{n1}+m_2-1} + An_2 r^{\beta_{n2}+m_2-1}\right]\right\}
\end{aligned} \tag{23}$$

Eqs. (23) are system ordinary differential equation having general and particular solution. The general solution are assumed as

$$u_n^g(r) = Dr^{\eta}, \qquad v_n^g(r) = Er^{\eta} \tag{24}$$

Substituting Eqs. (24) into Eqs. (23) yields:

$$\begin{aligned}
&\left[\eta(\eta-1)+(m_4+1)\eta+\left(\frac{(m_4+1)\bar{C}_{12}-\bar{C}_{22}-n^2\bar{C}_{66}}{\bar{C}_{11}}\right)\right]D+i\left[\left(\frac{\bar{C}_{12}+\bar{C}_{66}}{\bar{C}_{11}}\right)\eta+\frac{m_4\bar{C}_{12}-\bar{C}_{22}-\bar{C}_{66}}{\bar{C}_{11}}\right]nE=0\\
&\left[\eta(\eta-1)+(m_4-1)\eta-\left((m_4+1)+\frac{n^2\bar{C}_{22}}{\bar{C}_{66}}\right)\right]E+i\left[\left(\frac{\bar{C}_{12}}{\bar{C}_{66}}+1\right)\eta+\left((m_4+1)+\frac{\bar{C}_{12}}{\bar{C}_{66}}\right)\right]nD=0
\end{aligned} \tag{25}$$

A nontrivial solution is obtained by setting the determinant of the coefficients of Eqs. (25) equal to zero, a four order polynomial characteristic equations is obtained and it gives four eigen values η_{n1} to η_{n4}.

$$\begin{aligned}
&\left[\eta(n-1)+(m_4+1)\eta+\left(\frac{(m_4+1)\bar{C}_{12}-\bar{C}_{22}-n^2\bar{C}_{66}}{\bar{C}_{11}}\right)\right]\left[\eta(\eta-1)+(m_4+1)\eta-\left((m_4+1)+\frac{n^2\bar{C}_{22}}{\bar{C}_{66}}\right)\right]\\
&\quad+n^2\left[\left(\frac{\bar{C}_{12}+\bar{C}_{66}}{\bar{C}_{11}}\right)\eta+\frac{m_4\bar{C}_{12}-\bar{C}_{22}-\bar{C}_{66}}{\bar{C}_{11}}\right]\left[\left(\frac{\bar{C}_{12}}{\bar{C}_{66}}+1\right)\eta+\left((m_4+1)+\frac{\bar{C}_{12}}{\bar{C}_{66}}\right)\right]=0
\end{aligned} \tag{26}$$

Thus, the general solutions are

$$u_n^g(r) = \sum_{j=1}^{4} D_{nj} r^{\eta_{nj}}, \qquad v_n^g(r) = \sum_{j=1}^{4} N_{nj} D_{nj} r^{\eta_{nj}} \tag{27}$$

where N_{nj} is the relation between constant D_{nj} and E_{nj} is obtained from the of Eqs. (25) and they are presented at Appendix - part A. The particular solutions $u_n^p(r)$ and $v_n^p(r)$ are assumed as

$$\begin{aligned}
u_n^p(r) &= I_{n1} r^{\beta_{n_1}+m_2+1} + I_{n2} r^{\beta_{n_2}+m_2+1}\\
v_n^p(r) &= I_{n3} r^{\beta_{n_1}+m_2+1} + I_{n4} r^{\beta_{n_2}+m_2+1}
\end{aligned} \tag{28}$$

Substituting Eqs. (27) to non-homogeneous form of Eqs. (23) gives I_{n1} to I_{n4} as they are presented at Appendix –part A. The complete solutions for $u_n(r)$ and $v_n(r)$ are the sum of the general and particular solutions and are

$$\begin{aligned}
u_n(r) &= \sum_{j=1}^{4} D_{nj} r^{\eta_{nj}} + I_{n1} r^{\beta_{n1}+m_2+1} + I_{n2} r^{\beta_{n2}+m_2+1}\\
v_n(r) &= \sum_{j=1}^{4} N_{nj} D_{nj} r^{\eta_{nj}} + I_{n3} r^{\beta_{n1}+m_2+1} + I_{n4} r^{\beta_{n2}+m_2+1}
\end{aligned} \tag{29}$$

For $n=0$ the coefficient N_{nj} is undefined because the system of Eqs. (23) for $n=0$ is two decoupled ordinary differential equations as

$$u_0'' + (m_4+1)\frac{1}{r}u_0' + \left(\frac{(m_4+1)\bar{C}_{12} - \bar{C}_{22}}{\bar{C}_{11}}\right)\frac{1}{r^2}u_0 = \left[\left((m_2+m_4-1) - \frac{2\bar{C}_{12}}{\bar{C}_{11}}\right)\alpha_{01} + \left(\frac{2(m_2)m_4+1)\bar{C}_{12} + \bar{C}_{22}}{\bar{C}_{11}}\right)\alpha_{02}\right]$$
$$\left[A_{01}r^{\beta_{01}+m_2-1} + A_{02}r^{\beta_{02}+m_2-1} + \alpha_{01} + \frac{2\bar{c}_{12}}{\bar{c}_{11}}\alpha_{02}\right]\left[\beta_{01}A_{01}r^{\beta_{01}+m_{2-1}} + \beta_{02}A_{02}r^{\beta_{02}+m_{2-1}}\right]v_0''$$
$$+ (m_4+1)\frac{1}{r}v_0' - (m_4+1)\frac{1}{r^2}v_0 = 0 \tag{30}$$

This is the system of Euler differential equations. Thus, the solution of homogeneous part of Eqs. (30) may be assumed in the form

$$u_0^g(r) = D_0 r^{\eta_0}, \qquad v_0^g(r) = E_0 r^{\eta_0} \tag{31}$$

where D_0, E_0 and η_0 are constants to be found using the given boundary conditions. Substituting Eqs. (31) into the homogeneous parts of Eqs. (30) yields:

$$\left[\eta_0(\eta_0-1) + (m_4+1)\eta_0 + \left(\frac{(m_4+1)\bar{C}_{12} - \bar{C}_{22}}{\bar{C}_{11}}\right)\right] = 0$$
$$\eta_0(\eta_0-1) + (m_4+1)\eta_0 - (m_4+1) = 0 \tag{32}$$

Thus, the general solution is:

$$u_{\circ}(r) = \sum_{j=1}^{2} D_{oj}r^{\eta_{oj}} + I_{oj}r^{\beta_{0j}+m_1+1}$$
$$v_o(r) = \sum_{j=3}^{4} D_{oj}\ r^{\eta_{oj}} \tag{33}$$

Substituting Eqs.(29) and (35) into Eqs.(22) give

$$u(r,\theta) = \sum_{j=1}^{2}(D_{oj}r^{\eta_{oj}} + I_{oj}r^{\beta_{oj}+m_2+1}) + \sum_{\substack{n=-\infty \\ n\neq 0}}^{\infty}\left[\sum_{j=1}^{4} D_{nj}r^{\eta_{nj}} + I_{n1}r^{\beta_{n1}+m_2+1} + I_{n2}r^{\beta_{n2}+m_2+1}\right]\mathrm{e}^{in\theta}$$
$$v(r,\theta) = \sum_{j=3}^{4} D_{oj}r^{\eta_{oj}} + \sum_{\substack{n=-\infty \\ n\neq 0}}^{\infty}\left[\sum_{j=1}^{4} N_{nj}D_{nj}r^{\eta_{nj}} + I_{n3}r^{\beta_{n1}+m_2+1} + I_{n4}r^{\beta_{n2}+m_2+1}\right]\mathrm{e}^{in\theta} \tag{34}$$

Substituting Eqs. (34) into Eqs. (11) the strains intensity are obtained as

$$\varepsilon_{rr} = \sum_{j=1}^{2}\eta_{oj}D_{oj}r^{\eta_{oj}-1} + (\beta_{o1}+m_2+1)I_{oj}r^{\beta_{oj}+m_2} + \sum_{\substack{n=-\infty \\ n\neq 0}}^{\infty}[\sum_{j=1}^{4}\eta_{nj}D_{nj}r^{\eta_{nj}-1} + I_{n_1}(\beta_{n1}+m_2+1)r^{\beta_{n1}+m_2} + +I_{n2}(\beta_{n2}+m_2+1)r^{\beta_{n2}+m_2}]e^{in\theta}$$
$$\varepsilon_{\theta\theta} = \sum_{j=1}^{2}D_{oj}r^{\eta_{oj}} + I_{oj}r^{\beta_{0j}+m_2} + \sum_{\substack{n=-\infty \\ n\neq 0}}^{\infty}[\sum_{j=1}^{4}(inN_{nj}+1)D_{nj}r^{\eta_{nj}-1} + (inI_{n_3}+I_{n1})r^{\beta_{n_1}+m_2} + (inI_{n4}+I_{n2})r^{\beta_{n2}+m_2}]e^{in\theta}$$
$$\varepsilon_{r\theta} = \frac{1}{2}\sum_{j=1}^{2}(\eta_{oj}-1)D_{oj}r^{\eta_{oj}} + \sum_{\substack{n=-\infty \\ n\neq 0}}^{\infty}[\sum_{j=1}^{4}(in+(\eta_{nj}-1)N_{nj})D_{nj}r^{\eta_{nj}-1} + (inI_{n1}+(\beta_{n1}+m_2)I_{n3})r^{\beta_{n1}+m_2} + (inI_{n2}+(\beta_{n2}+m_2)I_{n4})r^{\beta_{n2}+m_2}]e^{in\theta} \tag{35}$$

Substituting Eqs. (35) into Eqs. (16) the stresses are obtained as

$$\begin{aligned}
\sigma'_{rr} &= \sum_{j=1}^{2}\Big[\eta_{oj}D_{oj}r^{\eta_{oj}-1}+(\beta_{oj}+m_2+1)I_{oj}r^{\beta_{oj}+m_2}+(H_1)D_{0j}r^{\eta_{oj}}+I_{oj}r^{\beta_{0j}+m_2}\Big] \\
&\quad+\Bigg[\sum_{\substack{n=-\infty\\ n\neq 0}}^{\infty}\Bigg(\sum_{j=1}^{4}\eta_{nj}D_{nj}r^{\eta_{nj}-1}+I_{n_1}(\beta_{n1}+m_2+1)r^{\beta_{n1}+m_2}+I_{n2}(\beta_{n2}+m_2+1)r^{\beta_{n2}+m_2} \\
&\quad+H_1\Big[(inN_{nj}+1)D_{nj}r^{\eta_{nj}-1}+(inI_{n_3}+I_{n1})r^{\beta_{n_1}+m_2}+(inI_{n4}+I_{n2})r^{\beta_{n2}+m_2}\Big]-\Big[(\alpha_{01}+2H_1\alpha_{02})(A_{n1}r^{\beta_{n1}+m_2+m_4}+A_{n2}r^{\beta_{n2}+m_2+m_4})\Big]\Bigg]\ e^{in\theta} \\
\sigma'_{\theta\theta} &= \sum_{j=1}^{2}\Big[(D_{0j}r^{\eta_{oj}}+I_{oj}r^{\beta_{0j}+m_2})+(H_2)\eta_{oj}D_{oj}r^{\eta_{oj}-1}(\beta_{o1}+m_2+1)I_{oj}r^{\beta_{oj}+m_2}\Big] \\
&\quad+\Bigg[\sum_{\substack{n=-\infty\\ n\neq 0}}^{\infty}\Bigg(\sum_{j=1}^{4}(inN_{nj}+1)D_{nj}r^{\eta_{nj}-1}\Bigg)+(inI_{n_3}+I_{n1})r^{\beta_{n1}+m_2} \\
&\quad+(H_2)\Big[\eta_{nj}D_{nj}r^{\eta_{nj}-1}+I_{n_1}(\beta_{n1}+m_2+1)r^{\beta_{n1}+m_2}+I_{n2}(\beta_{n2}+m_2+1)r^{\beta_{n2}+m_2}\Big] \\
&\quad-\Big[(2H_2\alpha_{01}+\alpha_{02})(A_{n1}r^{\beta_{n1}+m_2+m_4}+A_{n2}r^{\beta_{n2}+m_2+m_4})\Big]\Bigg]e^{in\theta} \\
\sigma'_{r\theta} &= \sum_{j=1}^{2}(\eta_{oj}-1)D_{oj}r^{\eta_{oj}}+2\sum_{\substack{n=-\infty\\ n\neq 0}}^{\infty}\sum_{j=1}^{4}\Big[(in+(\eta_{nj}-1)N_{nj})D_{nj}r^{\eta_{nj}-1}+(inI_{n1}+(\beta_{n1}+m_2)I_{n3})r^{\beta_{n1}+m_2}+(inI_{n2}+(\beta_{n2}+m_2)I_{n4})r^{\beta_{n2}+m_2}\Big]\mathrm{e}^{in\theta}
\end{aligned} \tag{36}$$

where

$$H_1=\frac{\bar{C}_{12}}{\bar{C}_{11}},\qquad H_2=\frac{\bar{C}_{12}}{\bar{C}_{22}},\qquad \sigma'_{rr}=\frac{\sigma_{rr}}{\bar{C}_{11}},\qquad \sigma'_{\theta\theta}=\frac{\sigma_{\theta\theta}}{\bar{C}_{22}},\qquad \sigma'_{r\theta}=\frac{\sigma_{r\theta}}{\bar{C}_{66}} \tag{37}$$

To determine the constants D_{nj}, we may consider any general form of boundary for displacement and stresses as

$$\begin{aligned}
&u(a,\theta)=w_1(\theta) && \sigma_{rr}(a,\theta)=w_5(\theta)\\
&u(b,\theta)=w_2(\theta) && \sigma_{rr}(b,\theta)=w_6(\theta)\\
&v(a,\theta)=w_3(\theta) && \sigma_{r\theta}(a,\theta)=w_7(\theta)\\
&v(b,\theta)=w_4(\theta) && \sigma_{r\theta}(b,\theta)=w_8(\theta)
\end{aligned} \tag{38}$$

Expanding the given boundary conditions in complex Fourier series gives

$$w_j(\theta)=\sum_{n=-\infty}^{\infty}W_j(n)\ \mathrm{e}^{in\theta},\qquad j=1,...,4 \tag{39}$$

where

$$W_j(n)=\frac{1}{2\pi}\int_{-\pi}^{\pi}w_j(n)\ \mathrm{e}^{in\theta}\mathrm{d}\theta,\qquad j=1,...,4 \tag{40}$$

Using the selected six boundary conditions of Eqs. (38) with help of Eqs. (39) and (40) four unknown coefficients D_{n1} to D_{n4} are calculated.

3 RESULTS AND DISCUSSION

Consider a thick hollow cylinder of inner radius $a=1(\mathrm{m})$ and outer radius $b=1.2(\mathrm{m})$ shown properties are given in Table 1. For simplicity of analysis, we consider the power law of material properties be the same as $m_1=m_2=m_3=m_4=m.$ To examine the proposed solution method, two example problems are considered. The first example problem may have some physical interpretation, while the second example is chosen to show the mathematical effectiveness of the proposed method .The first example problem may have some physical interpretation, while the second example is chosen to show the mathematical effective of the proposed method. As the first example, consider a thick hollow cylinder where the inside boundary is traction –free with given temperature distribution of the Table1.The outside boundary is assumed to be radially fixed with zero temperature. Therefore, the assumed boundary conditions yield of the Table 1. The thermal boundary conditions are obtained and the temperature is distributed, where the constants of integration are obtained from in Appendix –part B. In general, the displacement and stress boundary conditions are substituted in Eqs. (34) and with proper function expansions (35) the constant coefficients of the series expansions are obtained from Eqs. (36). B is compressibility coefficient, sometimes called the Skempton pore pressure coefficient and ϕ is pore volume fraction is pore per unite total volume, respectively, are given in Appendix – part B. To examine the proposed solution method two example problems are considered.

The first example problem may have some physical interpretation, while the second example is chosen to show the mathematical effectiveness of the proposed method. As the first example, consider a thick hollow cylinder where the inside boundary is traction –free with given temperature distribution of the Table 2.The outside boundary is assumed to be radially fixed with zero temperature. Therefore, the assumed boundary conditions yield of the Table 2.

As the second example, a thick-walled cylinder may be assumed with zero temperature distribution and but exposed to mechanical boundary conditions. The stress and displacement boundary conditions are assumed of the Table3.The reason to select such boundary condition is to examine the mathematical strength of proposed method. These types of boundary conditions may not be handled with the potential function method. It is to examined that expansion of Eq. (36) rapidly converge after 31 number of terms .Therefore, in the calculation and plotting the Figures, 31 terms of each series are considered. Using Eqs. (34) to (36) the boundary conditions given in radial stress and electric potential in Table 3 are expanded by the integral series and the unknown coefficients D_{nj} are determined. Fig. 1 shows the temperature distribution in the wall thickness along the radius and circumferential directions. The effect of the power-law index on the distribution of the temperature radial is shown in Figs. 2 and 3 shows the resulting thermoelastic radial displacement due to the given temperature variations. The effect of the power-law index on the radial displacement versus *r/a* is shown in Fig. 4.

Table 1
Material property [3]

	E (GPa)	γ	ν	ν_u	$\alpha_0(1/^\circ\mathrm{c})$
Material 1	200	0.47	0.2	0.3	0.000012

Table 2
Boundary conditions

$T(a,\theta)$	$\sigma_{rr}(a,\theta)$	$\sigma_{r\theta}(a,\theta)$	$u(b,\theta)$	$v(b,\theta)$
$60\sin(2\theta)$ $(^\circ\mathrm{c})$	0	0	0	0

Table 3
Boundary conditions

$T(a,\theta)$	$T(b,\theta)$	$\sigma_{rr}(a,\theta)$	$\sigma_{r\theta}(a,\theta)$	$u(b,\theta)$	$v(b,\theta)$
0	**0**	$200\cos\left(\frac{\theta^2}{4}-\theta\right)$ (MPa)	$50\theta^2\sin(\theta)$ (MPa)	**0**	**0**

The resulting circumferential displacement v is shown in Fig. 5. Due to the assumed boundary conditions, it is noted that, the u and v-displacement are zero at $r=b$ and follow the pattern of the temperature distribution inside surface at $r/a=1$. The effect of the power-law index on the circumferential displacement relate of r/a is shown in Figs. 6, 7, 9 and 11 show the of the radial, circumferential, and, the shear thermal stress in the cross section of the cylinder. It is interesting to see that all components of stresses follow a harmonic pattern on the outside surface .The radial and shear stresses are zero at the insider surface, due to the assumed boundary conditions. The effect of the power-law index on the distribution of the radial, Hoop and Shear thermal stress is shown in Figs.8, 10 and 12 respectively. This Figure is the plot of stresses versus r/a at $\theta = \pi / 3$. It is shown as m increases, the radial, hoop and shear thermal stress is increased. Figs. 13, 15 and 17 show the radial, hoop and shear thermal stresses in the cross section of the cylinder respectively where the pore compressibility coefficient (B) is changed the other parameters are fixed. Figs. 14, 16 and 18 show these stresses based on the pore volume fraction (ϕ) is pore volume per total volume. Figs. 19 and 21 show the radial and circumferential displacements in the cross section of the cylinder respectively based on the pore compressibility coefficient (B) changing. Figs. 20 and 22 also show these displacement based on the pore volume fraction (ϕ) changing. Figs. 23 and 25 show the radial and circumferential displacements in the cross section of the cylinder.

According to the boundary conditions, we have $u=v=0$ at $r=b$. At the inside surface $r=a$, u and v are harmonically varying. The effect of the power-law index on the radial and circumferential displacement relate of r/a is shown in Figs. 24 and 26. The stress distribution is shown in Figs. 27, 29 and 31. Stress patterns in inside and outside surfaces follow harmonic patterns. The given harmonic boundary conditions for σ_{rr} and $\sigma_{r\theta}$ at $r=a$, have general influence on the pattern of stress distributions in the cylinders cross section, as seen from Figs. 27 through 31. The effect of the power-law index on the distribution of the radial, hoop and shear thermal stress is shown in Figs. 28, 30 and 32, respectively. This Figure is the plot of stresses versus r/a at $\theta = \pi / 3$. It is shown that as m increases, the radial, hoop and shear thermal stress is increased. Figs 33, 35, and 37 show the radial, hoop and shear thermal stresses in the cross section of the cylinder respectively where the pore compressibility coefficient (B) is changed the other parameters are fixed. Figs. 34, 36, and 38 show these stresses based on the pore volume fraction (ϕ) is pore volume per total volume. Figs.39 and 41 show the variations of the radial and circumferential displacements in the cross section of the cylinder respectively based on the pore compressibility coefficient (B) changing. Figs .40 and 42 also show these displacements based on the pore volume fraction (ϕ) changing.

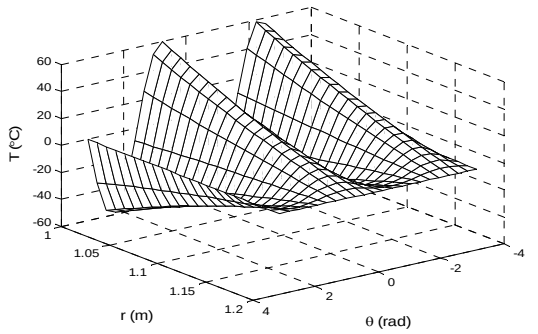

Fig. 1
Temperature distribution in the cross section of cylindrical.

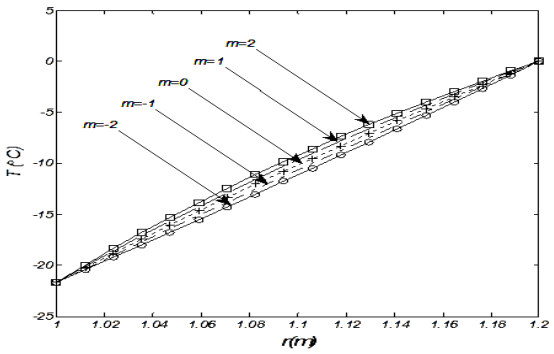

Fig. 2
Temperature distribution of radial at $\theta = \pi / 3$.

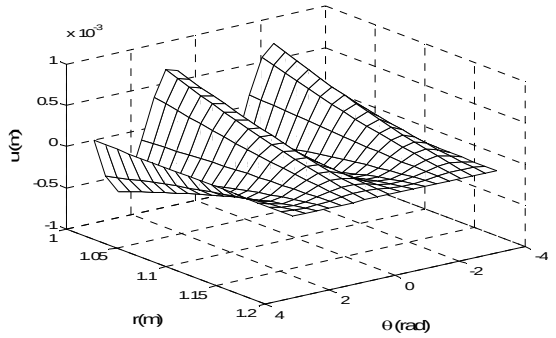

Fig. 3
Radial displacement in the cross section of cylindrical.

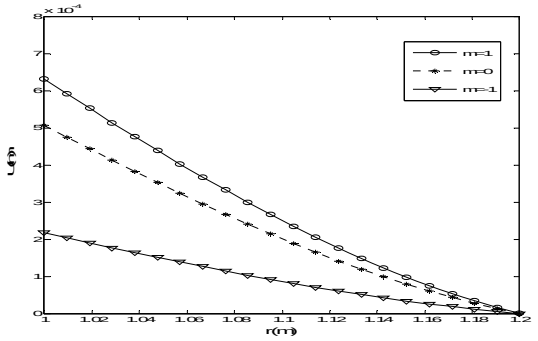

Fig. 4
Radial displacement relate of *r*/*a* at $\theta = \pi / 3$.

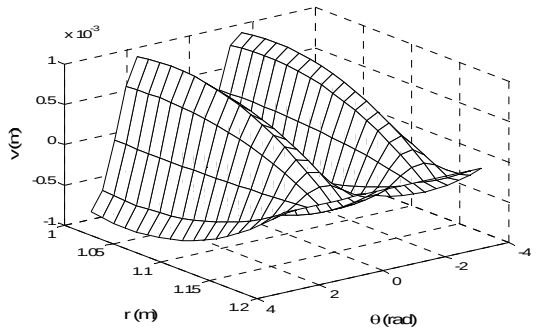

Fig. 5
Circumferential displacement in the cross section of cylindrical.

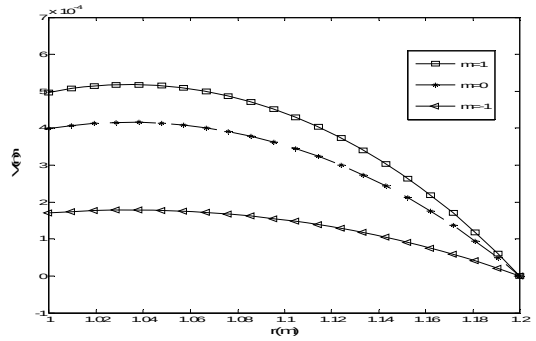

Fig. 6
Circumferential displacement relate of radial at $\theta = \pi / 3$.

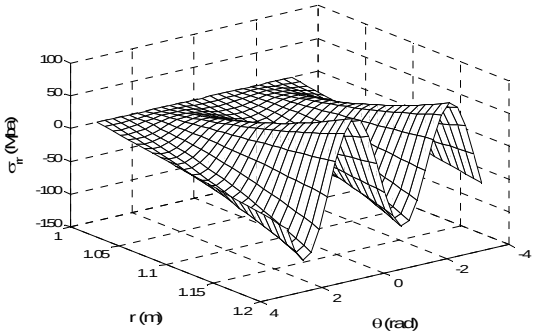

Fig. 7
Radial thermal stress in the cross section of cylindrical.

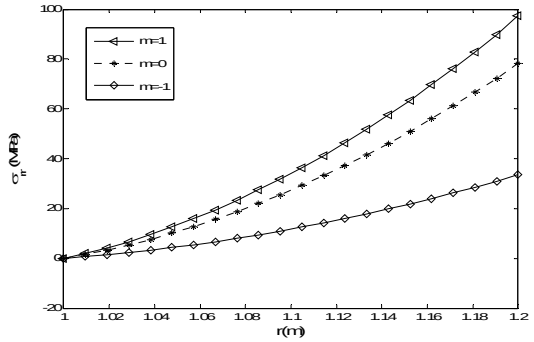

Fig. 8
Radial distribution of radial thermal stress σ_{rr} at $\theta = \pi / 3$.

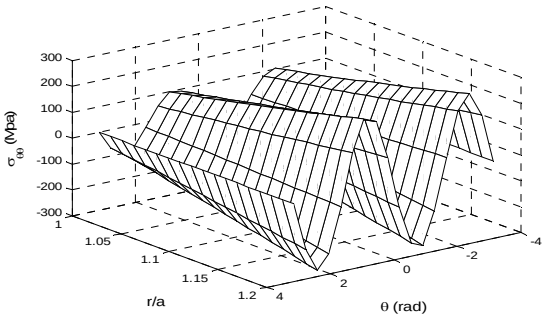

Fig. 9
Hoop thermal stress in the cross section of cylindrical.

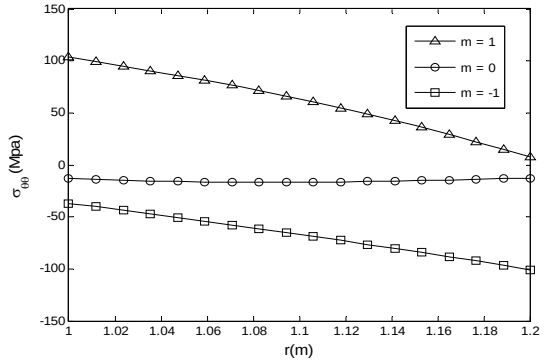

Fig. 10
Hoop distribution of radial thermal stress $\sigma_{\theta\theta}$ at $\theta = \pi / 3$.

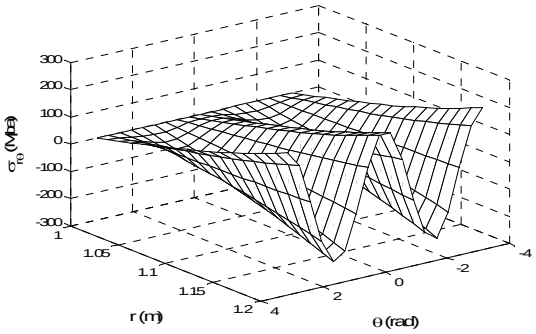

Fig. 11
Shear thermal stress in the cross section of cylindrical**.**

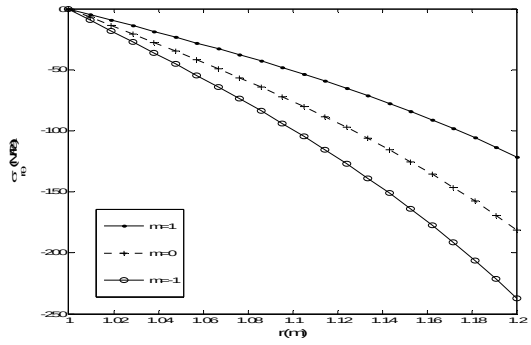

Fig. 12
Shear distribution of radial thermal stress $\sigma_{r\theta}$ at $\theta = \pi / 3$.

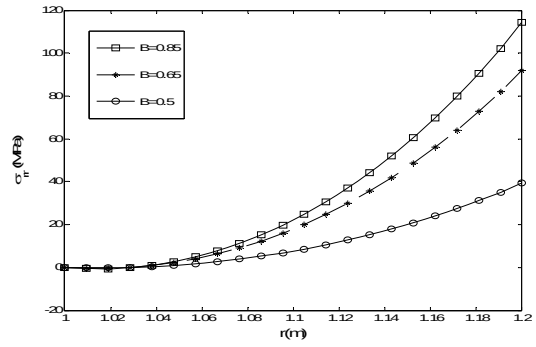

Fig. 13
Radial thermal stress in the cross section of cylindrical based on the compressibility coefficient (B) changing.

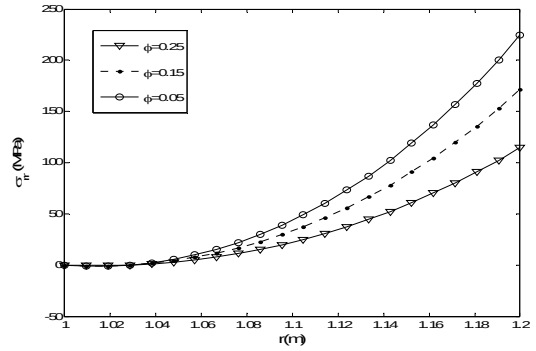

Fig. 14
Radial thermal stress in the cross section of cylindrical based on the pore volume fraction (ϕ) changing.

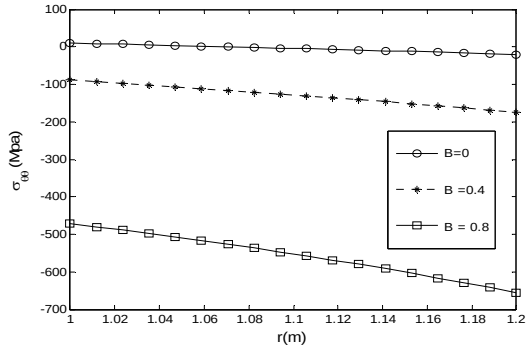

Fig. 15
Hoop thermal stress in the cross section of cylindrical based on the compressibility coefficient (B) changing.

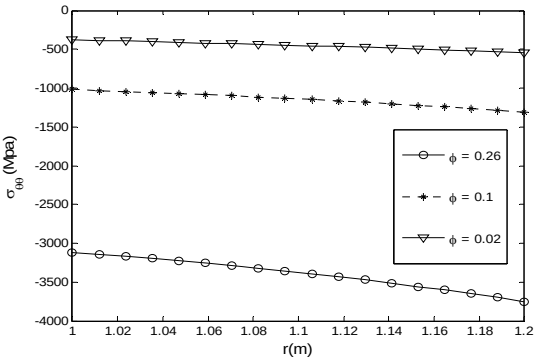

Fig.16
Hoop thermal stress in the cross section of cylindrical based on the pore volume fraction (ϕ) changing.

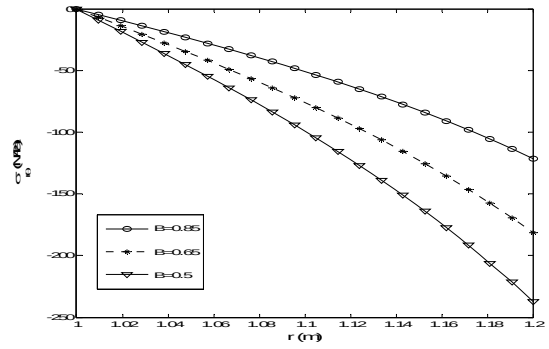

Fig. 17
Shear thermal stress in the cross section of cylindrical based on the compressibility coefficient (B) changing.

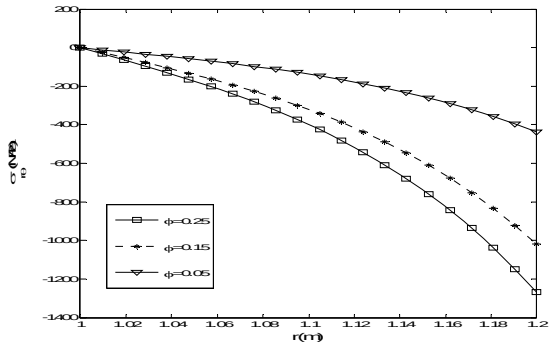

Fig. 18
Shear thermal stress in the cross section of cylindrical based on the pore volume fraction (ϕ) changing.

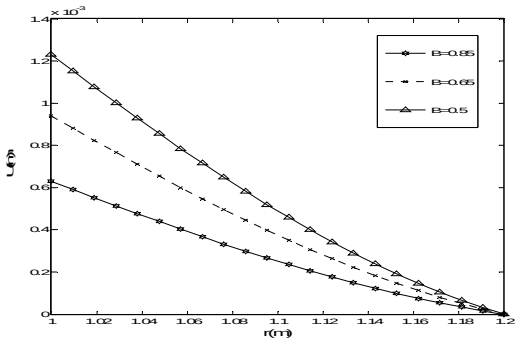

Fig. 19
Radial displacement in the cross section of cylindrical based on the compressibility coefficient (B) changing.

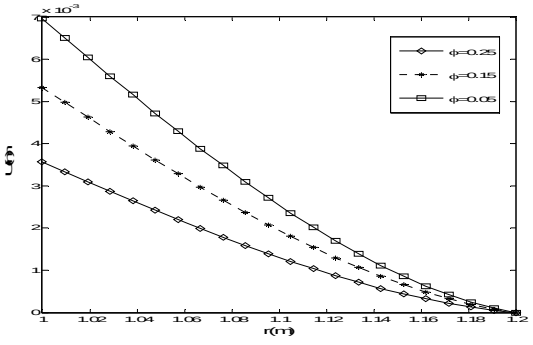

Fig. 20
Radial displacement in the cross section of cylindrical based on the pore volume fraction (ϕ) changing.

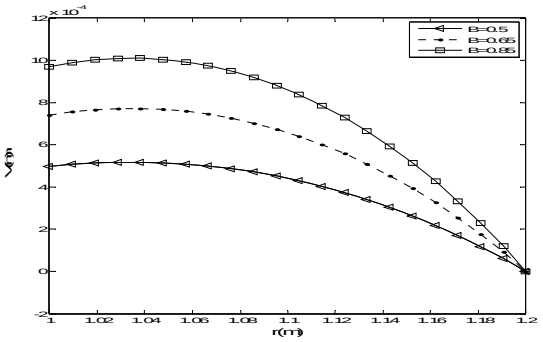

Fig. 21
Circumferential displacement in the cross section of cylindrical based on the compressibility coefficient (B) changing.

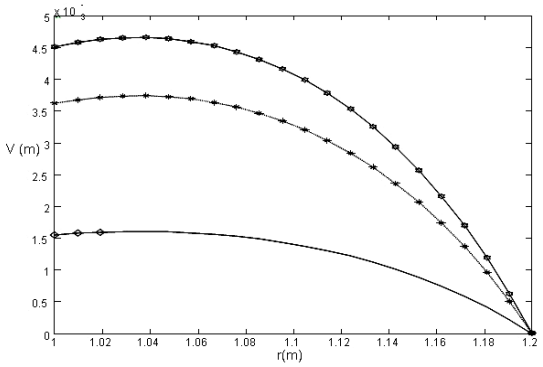

Fig. 22
Circumferential displacement in the cross section of cylindrical based on the pore volume fraction (ϕ) changing.

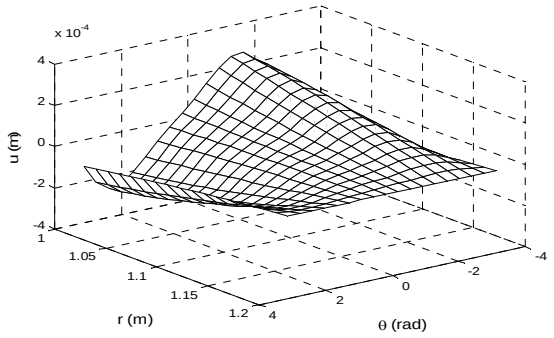

Fig. 23
Radial displacement in the cross section of cylindrical.

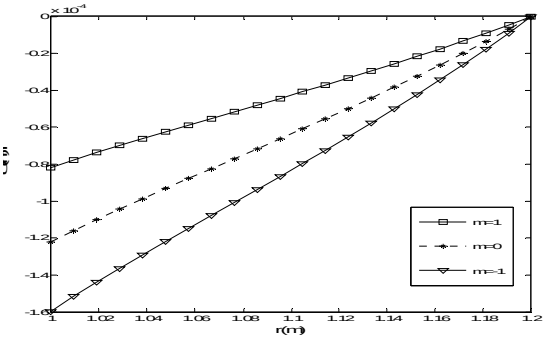

Fig. 24
Radial displacement relate of *r*/*a* at $\theta = \pi / 3$.

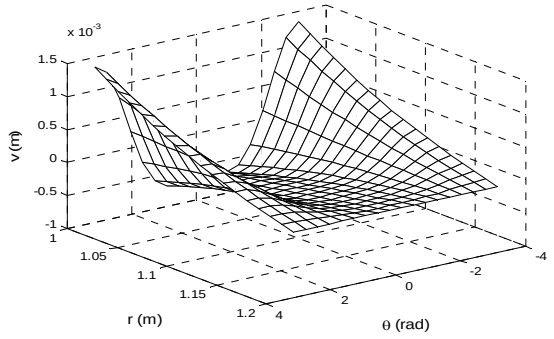

Fig. 25
Circumferential displacement in the cross section of cylindrical.

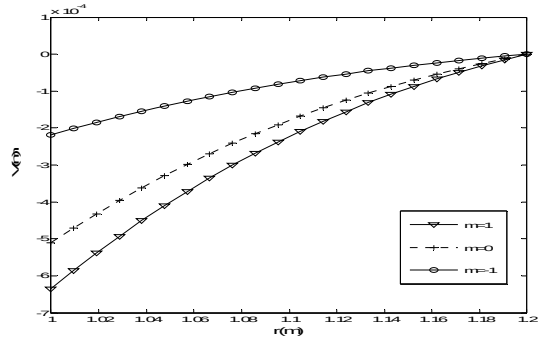

Fig. 26
Circumferential displacement relate of radial at $\theta = \pi / 3$.

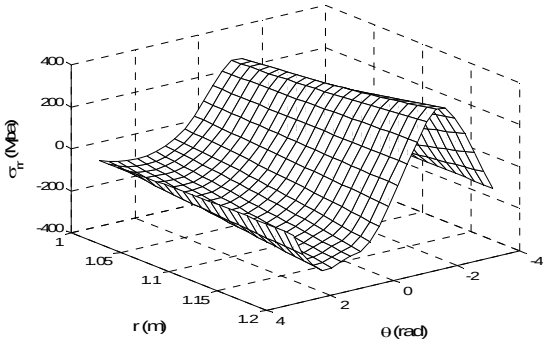

Fig.27
Radial thermal stress in the cross section of cylindrical.

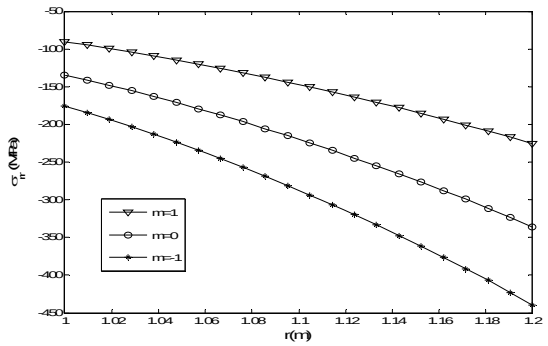

Fig.28
Radial distribution of radial thermal stress σ_{rr} at $\theta = \pi / 3$.

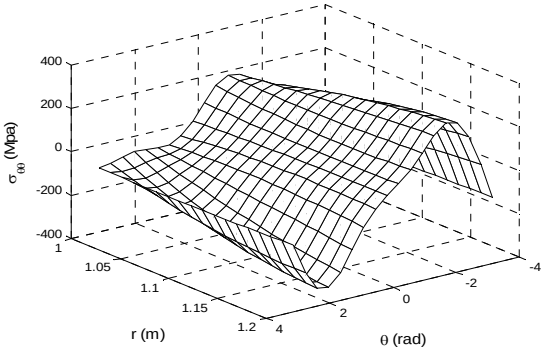

Fig.29
Hoop thermal stress in the cross section of cylindrical.

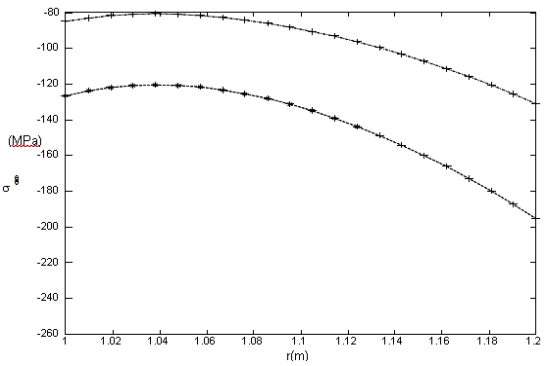

Fig.30
Hoop distribution of radial thermal stress $\sigma_{\theta\theta}$ at $\theta = \pi / 3$.

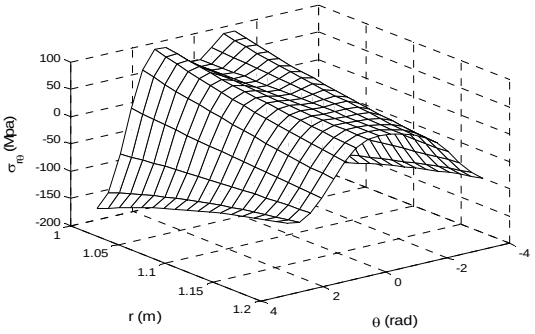

Fig. 31
Shear thermal stress in the cross section of cylindrical.

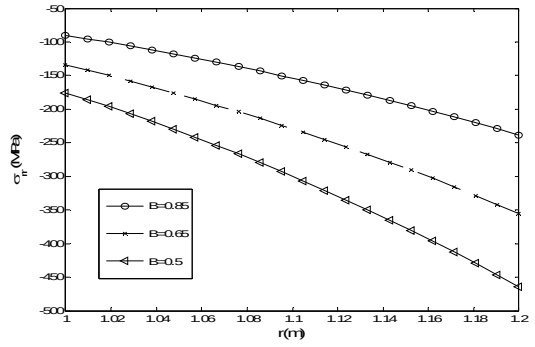

Fig. 33
Radial thermal stress in the cross section of cylindrical based on the compressibility coefficient (B) changing.

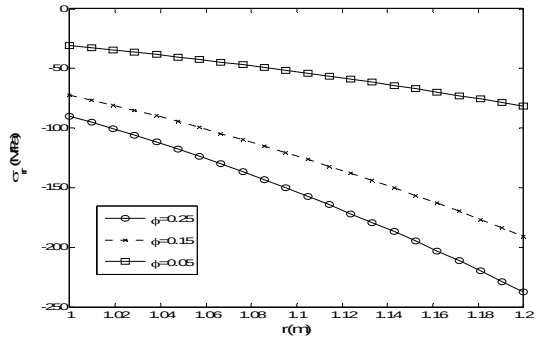

Fig. 34
Radial thermal stress in the cross section of cylindrical based on the pore volume fraction (ϕ) changing.

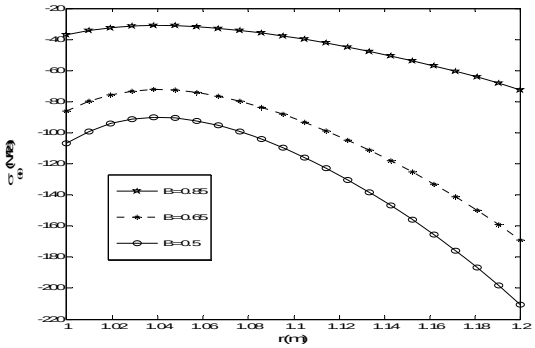

Fig. 35
Hoop thermal stress in the cross section of cylindrical based on the compressibility coefficient (B) changing.

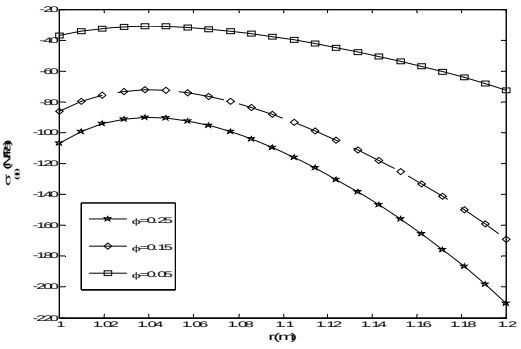

Fig. 36
Hoop thermal stress in the cross section of cylindrical based on the pore volume fraction (ϕ) changing.

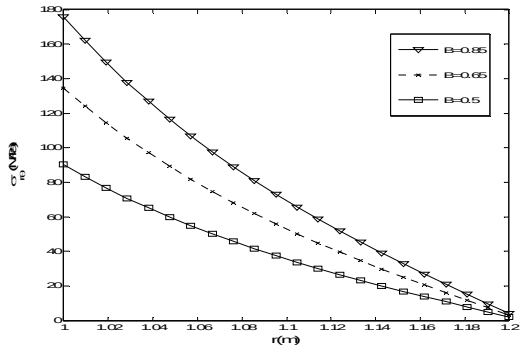

Fig. 37
Shear thermal stress in the cross section of cylindrical based on the compressibility coefficient (B) changing.

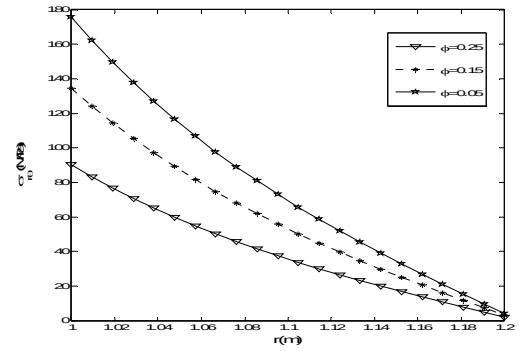

Fig. 38
Shear thermal stress in the cross section of cylindrical based on the pore volume fraction (ϕ) changing.

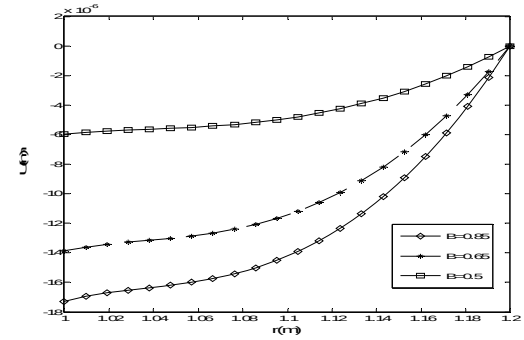

Fig. 39
Radial displacement in the cross section of cylindrical based on the compressibility coefficient (B) changing.

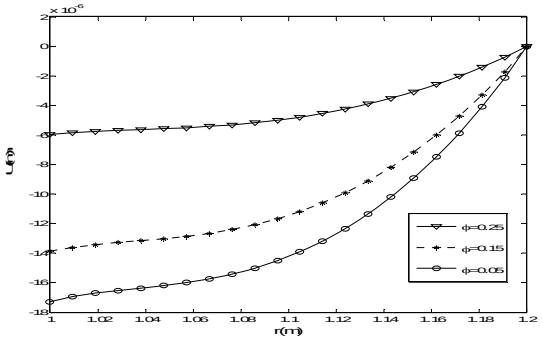

Fig. 40
Radial displacement in the cross section of cylindrical based on the pore volume fraction (ϕ) changing.

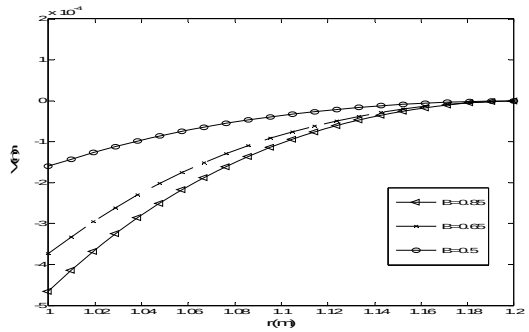

Fig. 41
Circumferential displacement in the cross section of cylindrical based on the compressibility coefficient (B) changing.

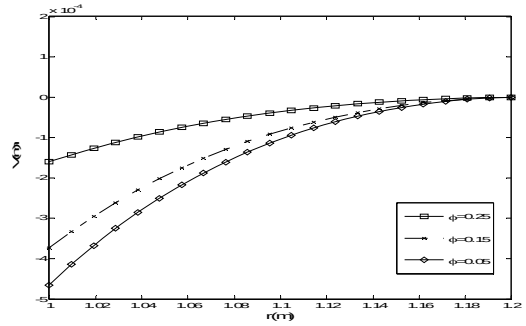

Fig. 42
Circumferential displacement in the cross section of cylindrical based on the pore volume fraction (ϕ) changing.

4 CONCLUSIONS

In the present, work an attempt has been made to study the problem of general solution for the thermal and mechanical stresses in a thick FGPM hollow cylinder due to the two-dimensional non-axissymmmetric steady-state loads. The method of solution is based on the direct method and uses power series, rather than the potential function method. The advantage of this method is its mathematical power to handle both simple and complicated mathematical function for the thermal and mechanical stresses boundary conditions. The potential function method is capable of handling complicated mathematical functions as boundary condition. The proposed method does not have the mathematical limitations to handle the general types of boundary conditions which are usually countered in the potential function method.

APPENDICES

Appendix A

$$u_n(r)=\frac{1}{2\pi}\int_{-\pi}^{\pi}u(r,\theta)e^{-in\theta}\mathrm{d}\theta,\qquad v_n(r)=\frac{1}{2\pi}\int_{-\pi}^{\pi}v(r,\theta)e^{-in\theta}\mathrm{d}\theta$$

$$N_{nj}=\frac{\left[\eta_{nj}(\eta_{nj}-1)+(m_1+1)\eta_{nj}+\frac{m_1(\nu+\nu_u-4\nu\nu_u}{1-\nu-\nu_u}-1-\frac{(1-2\nu-2\nu_u+4\nu\nu_u)n^2}{2-2\nu-2\nu_u}\right]}{n\left[\frac{(1-4\nu\nu_u)\eta_{nj}}{2-2\nu-2\nu_u}+\frac{(2m_1)(\nu+\nu_u-4\nu\nu_u)+(4\nu+4\nu_u-4\nu\nu_u)-3}{2-2\nu-2\nu_u}\right]},\qquad j=1,2,3,4$$

$$e_1=\frac{1}{2\pi}\int_{-\pi}^{\pi}f_1(\theta)e^{-in\theta}\mathrm{d}\theta,\qquad e_2=\frac{1}{2\pi}\int_{-\pi}^{\pi}f_2(\theta)e^{-in\theta}\mathrm{d}\theta,\qquad e_3=(C_{11}a^{\beta_{n1}}+C_{12}\beta_{n1}a^{\beta_{n1}-1})$$

$$e_4=(C_{11}a^{\beta_{n2}}+C_{12}\beta_{n2}a^{\beta_{n2}-1}),\qquad e_5=(C_{21}b^{\beta_{n1}}+C_{22}\beta_{n1}b^{\beta_{n1}-1}),\qquad e_6=(C_{21}b^{\beta_{n2}}+C_{22}\beta_{n2}b^{\beta_{n2}-1})$$

$$\sum_{n=-\infty}^{\infty}[e_3a_n+e_4b_n]e^{in\theta}=f_1(\theta),\quad \sum_{n=-\infty}^{\infty}[e_5a_n+e_6b_n]e^{in\theta}=f_2(\theta),\quad e_3a_n+e_4b_n=e_1,\quad e_5a_n+e_6b_n=e_2$$

$$d_1D_{n1}+d_3D_{n3}=d_5,\qquad d_9D_{n1}+d_7D_{n3}=d_{11},\qquad d_2D_{n2}+d_4D_{n4}=d_6,\qquad d_{10}D_{n2}+d_8D_{n4}=d_{12}$$

$$D_{n1}=\frac{d_5d_7-d_3d_{11}}{d_1d_7-d_3d_9},\qquad D_{n2}=\frac{d_6d_8-d_4d_{12}}{d_2d_8-d_4d_{10}},\qquad D_{n3}=\frac{d_1d_{11}-d_5d_9}{d_1d_7-d_3d_9},\qquad D_{n4}=\frac{d_2d_{12}-d_6d_{10}}{d_2d_8-d_4d_{10}}$$

$$B=\frac{3(\upsilon_u-\upsilon)}{(1-2\upsilon)(1+\upsilon_u)},\qquad \phi=\frac{\gamma(B-k_f)}{B\left[(1-\alpha)+k\right]},\qquad 0\le B\le 1 \tag{A.1}$$

where k_f and k are bulk modulus of the fluid phase and bulk modulus of the poroelastic medium under the drained condition, respectively.

Appendix B

The constants d_j given as:

$$d_1=(\beta_{n1}+m_2+1)(\beta_{n1}+m_2)+(m_1+1)(\beta_{n1}+m_2+1)+\frac{(\nu+\nu_u-4\nu\nu_u)m_1}{1-\nu-\nu_u}-1-\frac{(1-2\nu-2\nu_u+4\nu\nu_u)n^2}{2-2\nu-2\nu_u}$$

$$d_2=(\beta_{n2}+m_2+1)(\beta_{n2}+m_2)+(m_1+1)(\beta_{n2}+m_2+1)+\frac{(\nu+\nu_u-4\nu\nu_u)m_1}{1-\nu-\nu_u}-1-\frac{(1-2\nu-2\nu_u+4\nu\nu_u)n^2}{2-2\nu-2\nu_u}$$

$$d_3=in\left(\frac{\beta_{n1}+m_2+1}{2-2\nu-2\nu_u}+\frac{(2m_1)(\nu+\nu_u-4\nu\nu_u)+(4\nu+4\nu_u-4\nu\nu_u)-3}{2-2\nu-2\nu_u}\right)$$

$$d_4=in\left(\frac{\beta_{n2}+m_2+1}{2-2\nu-2\nu_u}+\frac{(2m_1)(\nu+\nu_u-4\nu\nu_u)+(4\nu+4\nu_u-4\nu\nu_u)-3}{2-2\nu-2\nu_u}\right)$$

$$d_5=\frac{(1+\nu+\nu_u+4\nu\nu_u)(m_1+m_2+\beta_{n1})\alpha_0a_n}{1-\nu-\nu_u},\qquad d_6=\frac{(1+\nu+\nu_u+4\nu\nu_u)(m_1+m_2+\beta_{n2})\alpha_0b_n}{1-\nu-\nu_u}$$

$$d_7=(\beta_{n1}+m_2+1)(\beta_{n1}+m_2)+(m_1+1)(\beta_{n1}+m_2+1)-m_1-1-\frac{(2-2\nu-2\nu_u)n^2}{1-2\nu-2\nu_u+4\nu\nu_u}$$

$$d_8=(\beta_{n2}+m_2+1)(\beta_{n2}+m_2)+(m_1+1)(\beta_{n2}+m_2+1)-m_1-1-\frac{(2-2\nu-2\nu_u)n^2}{1-2\nu-2\nu_u+4\nu\nu_u}$$

$$d_9=in\left(\frac{\beta_{n1}+m_2+1}{1-2\nu-2\nu_u+4\nu\nu_u}+\frac{3-4\nu-4\nu_u+4\nu\nu_u}{1-2\nu-2\nu_u+4\nu\nu_u}+m_1\right)$$

$$d_{10}=in\left(\frac{\beta_{n2}+m_2+1}{1-2\nu-2\nu_u+4\nu\nu_u}+\frac{3-4\nu-4\nu_u+4\nu\nu_u}{1-2\nu-2\nu_u+4\nu\nu_u}+m_1\right)$$

$$d_{11}=\frac{in(2(1+\nu+\nu_u+4\nu\nu_u))\alpha_0a_n}{1-2\nu-2\nu_u+4\nu\nu_u},\qquad d_{12}=\frac{in(2(1+\nu+\nu_u+4\nu\nu_u))\alpha_0b_n}{1-2\nu-2\nu_u+4\nu\nu_u} \tag{B.1}$$

REFERENCES

[1] Lutz M.P., Zimmerman R.W., 1996, Thermal stresses and effective thermal expansion coefficient of functionally graded sphere, *Journal of Thermal Stresses* **19**: 39-54.

[2] Zimmerman R.W., Lutz M.P., 1999, Thermal stresses and thermal expansion in a uniformly heated functionally graded cylinder, *Journal of Thermal Stresses* **22**: 177-188.

[3] Jabbari M., Sohrabpour S., Eslami MR., 2003, General solution for mechanical and thermal stresses in functionally graded hollow cylinder due to radially symmetric loads, *ASME Journal of Applied Mechanics* **70**: 111-118.

[4] Poultangari R., Jabbari M., Eslami M.R., 2008, Functionally graded hollow spheres under non-axisymmetric thermo-mechanical loads, *International Journal of Pressure Vessels and Piping* **85**: 295-305.

[5] Shariyat M., Lavasani S.M.H., Khaghani M., 2009, Transient thermal stress and elastic wave propagation analyses of thick temperature-dependent FGM cylinders, using a second-order point-collocation method, *Applied Mathematical Modelling*, doi:10.1016/j.apm.2009.07.007.

[6] Lü C.F., Chen W.Q., Lim C.W., 2009, Elastic mechanical behavior of nano-scaled FGM films incorporating surface energies, *Composites Science and Technology* **69**: 1124-1130.

[7] Afsar A.M., Sekine H., 2002, Inverse problems of material distributions for prescribed apparent fracture toughness in FGM coatings around acircular hole in infinite elastic media, *Composites Science and Technology* **62**: 1063-1077.

[8] Zhang D.-G., Zhou Y.-H., 2008, A theoretical analysis of FGM thin plates based on physical neutral surface, *Computational Materials Science* **44**: 716-720.

[9] Fazelzadeh S.A.., Hosseini M., 2007, Aerothermoelastic behavior of supersonic rotating thin-walled beams made of functionally graded materials, *Journal of Fluids and Structures* **23**: 1251-1264.

[10] Ootao Y., Tanigawa Y., 2004, Transient thermoelastic problem of functionally graded thick strip due to non-uniform heat supply, *Composite Structures* **63**(2): 139-146.

[11] Jabbari M., Sohrabpour S., Eslami M.R., 2002, Mechanical and thermal stresses in a functionally graded hollow cylinder due to radially symmetric loads, *International Journal of Pressure Vessels and Piping* **79**: 493-497.

[12] Farid M., Zahedinejad P., Malekzadeh P., 2010, Three-dimensional temperature dependent free vibration analysis of functionally graded material curved panels resting on two-parameter elastic foundation using a hybrid semi-analytic, differential quadrature method, *Materials and Design* **31**: 2-13.

[13] Bagri A., Eslami M.R., 2008, Generalized coupled thermoelasticity of functionally graded annular disk considering the Lord–Shulman theory, *Composite Structures* **83**: 168-179.

[14] Samsam Shariat B.A., Eslami M.R., 2007, Buckling of thick functionally graded plates under mechanical and thermal loads, *Composite Structures* **78**: 433–439.

[15] Jabbari M., Bahtui A., Eslami MR., 2009, Axisymmetric mechanical and thermal stresses in thick short length functionally graded material cylinder, *International Journal of Pressure Vessels and Piping* **86**: 296-306.

[16] Thieme M., Wieters K.-P., Bergner F., Scharnweber D., Worch H., Ndop J., Kim T.J., Grill., 1999, Titanium powder sintering for preparation of a porous FGM Destined as a skeletal replacement implant, *Materials Science Forum* **308-311**: 374-382.

[17] Biot M.A., 1935, Le proble`me de la consolidation des matie`res argileuses sous une charge, *Annales de la Societe Scientifique de Bruxelles* B **55**: 110-113.

[18] Biot M.A.., 1941, General theory of three-dimensional consolidation, *Journal of Applied Physics* **12**: 155-164.

[19] De Boer R., 1996, Highlights in the historical development of the porous media theory: toward a consistent macroscopic theory, *Applied Mechanics Reviews* **49**: 201-262.

[20] Detournay E., Cheng A.H.-D., 1993, Fundamentals of Poroelasticity, in: *Comprehensive Rock Engineering: Principles, Practice and Projects*, edited by J.A. Hudson, Pergamon, Oxford, 113-171.

[21] Sandhu R.S., Wilson E.L., 1969, Finite element analysis of seepage in elastic media, *ASCE Journal of the Engineering Mechanics* **95**: 641-652.

[22] Detournay E., Cheng A.H.-D.,1993, Fundamentals of Poroelasticity, in: *Comprehensive Rock Engineering: Principles, Practice and Projects*, Chapter 5, vol. II, Analysis and Design Method, edited by C. Fairhurst, Pergamon Press, 113-171.

[23] Abousleiman Y., Ekboote S., 2005, solutions for inclined borehole in porothermoelastic transversely isotropic medium, *ASME Journal of Applied Mechanics* **72**(2): 102-114.

[24] Chen P.Y.P., 1980, Axismmetric thermal stresses in an anisotropic finite hollow cylinder, *Journal of Thermal Stresses* **6**(2-4): 197-205.

[25] Bai B., 2006, Fluctuation responses of saturated porous media subjected to cyclic thermal loading, *Computers and Geotechnics* **33**: 396-403.

[26] Wang Y., Papamichos E., 1994, An analytical solution for conductive heat flow and the thermally induced fluid flow around a wellbore in a poroelastic medium, *Water Resource Research* **36**(5): 3375-3384.

[27] Wang Y., Papamichos E., 1999, Thermal effects on fluid flow and hydraulic fracturing from wellbores and cavities in low-permeability formations, *International Journal for Numerical and Analytical Methods in Geomechanics* **23**(15): 1819-1834

[28] Ghassemi A., Tao Q., 2009, Influence of coupled chemo-poro-thermoelastic processes on pore pressure and stress distributions around a wellbore in swelling shale, *Journal of petroleum science and Engineering* **67**: 57-64

[29] Wirth B., Sobey I., 2006, An axisymmetric and fully 3D poroelastic model for the evolution of hydrocephalus, *Mathematical Medicine and Biology* **23**:363-388.

[30] Yang D., Zhang Z., 2002, Poroelastic wave equation including the Biot/squirt mechanism and the solid/fluid coupling anisotropy, *Wave Motion* **35**: 223-245

[31] Arora A., Tomar S.K., 2007, Elastic waves along a cylindrical borehole in a poroelastic medium saturated by two immiscible fluids, *Journal of Earth System Science* **116**(3): 225-234.

[32] Hamiel Y., Lyakhovsky V., Agnon A., 2004, Coupled evolution of damage and porosity in poroelastic media: theory and applications to deformation of porous rocks, *Geophysical Journal International* **156**: 701-713

[33] Ghassemi A., 2007, Stress and pore prepressure distribution around a pressurized, cooled crack in holw permeability rock, *Proceedings of the Thirty-Second Workshop on Geothermal Reservoir Engineering*, Stanford University, Stanford, California, January 22-24, SGP-TR-183

[34] Youssef H.M., 2007, Theory of generalized porothermoelasticity, *International Journal of Rock Mechanics & Mining Sciences* **44**: 222-227.

[35] Jourine S., Valkoo P.P., Kronenberg A.K., 2004, Modelling poroelastic hollow cylinder experiments with realistic boundary conditions, *International Journal for Numerical and Analytical Methods in Geomechanics* **28**: 1189-1205 (DOI: 10.1002/nag.383).